Double *K*-shell photoionization of neon

S. H. Southworth, E. P. Kanter, B. Krässig, and L. Young
Argonne National Laboratory, Argonne, Illinois 60439, USA

G. B. Armen and J. C. Levin
University of Tennessee, Knoxville, Tennessee 37996, USA

D. L. Ederer
Tulane University, New Orleans, Louisiana 70118, USA

M. H. Chen
Lawrence Livermore National Laboratory, Livermore, California 94550, USA
(Received 12 March 2003; published 24 June 2003)

Double *K*-shell photoionization of Ne at 5000 eV was observed by recording the *KK-KLL* Auger-electron hypersatellite spectrum. The measured Auger spectrum is compared with the results of multiconfiguration Dirac-Fock calculations. Shake calculations are used to identify likely multivacancy states produced by photoexcitation or ionization in addition to double-*K* vacancies, and their calculated Auger spectra are compared with the measured spectrum. The measured relative intensities of hypersatellite and diagram Auger lines are combined with experimental and theoretical determinations of branching ratios from single- and double-*K* vacancies into final states to determine the ratio of double-to-single *K*-shell photoionization cross sections to be 0.32(4)%. This ratio is much larger than the calculated high-energy-limit ratio and indicates a large contribution of dynamic electron correlation.

DOI: 10.1103/PhysRevA.67.062712 PACS number(s): 32.80.Fb, 32.80.Hd

I. INTRODUCTION

Double photoionization of He has been extensively studied as a probe of electron correlation in the simplest case of a two-electron system [1–3]. The many-body perturbation theory (MBPT) treatment [4] identifies three first-order amplitudes in the electron-electron interaction that are referred to as ground-state correlation (GSC), shakeoff (SO), and two-step-one (TS1) amplitudes. The GSC amplitude accounts for, e.g., angular and radial correlation between the two equivalent 1*s* electrons in the ground state [5]. Upon photoemission of one of the electrons, relaxation (or the sudden change in the average screening of the nuclear charge) can excite or eject the second electron and is described by the SO amplitude. The TS1 amplitude describes a process in which photoabsorption ejects one of the electrons and it undergoes a binary collision with the second electron and both are ejected. The three MBPT amplitudes provide intuitive descriptions of electron-electron interactions in the double photoionization process but should not be thought of as independent mechanisms and are added coherently in calculations of observables. Furthermore, the degree of importance of each amplitude changes depending on the choice of gauge form of the dipole operator, i.e., length, velocity, and acceleration [2–4,6]. However, a recent theoretical treatment describes double photoionization of He as an incoherent sum of SO and ''knockout'' (or TS1) contributions, with knockout calculated quasiclassically [7].

The same electron-electron interactions are expected to govern double *K*-shell photoionization in higher-*Z* atoms, with the energy variations of double-*K* photoionization cross sections following Z-scaling laws [8]. In the high-energy limit, the double-to-single *K*-shell photoionization cross-section ratio *R* can be accurately calculated for He and He-like ions [9,10], because electron-electron interaction in the final state is negligible and only ground-state correlation is needed. Accurate $1s^2$ ground-state wave functions can be constructed and the *Z* dependence of *R* in the asymptotic limit can be calculated. A good agreement exists between theory and the high-energy measurement (5.4–9.1 keV) on He using the ion-recoil momentum imaging method to distinguish photoabsorption from Compton scattering [11]. The energy required to reach the asymptotic limit scales as Z^2 [8]. At lower energies, *R* depends on dynamic correlation in the final state as described in the lowest order by TS1.

For atoms beyond He, *R* cannot be determined unambiguously from ion charge-state yields. However, double-*K* vacancy states can be identified by observing *KK-KL* hypersatellites in the x-ray fluorescence spectra [12–15] or *KK-KLL* hypersatellites in the Auger-electron spectra [16,17]. Experimental *R* values can be deduced from relative intensities of diagram and hypersatellite lines combined with the information on branching ratios into particular final states from initial single- and double-*K* vacancy states. In the present work, double-*K* photoionization of Ne at 5000 eV was observed by recording the *KK-KLL* Auger hypersatellite spectrum. The energies and transition rates of the hypersatellite spectrum have been calculated by Chen [18] using the multiconfiguration Dirac-Fock (MCDF) method. The measured Auger spectrum is complicated by contributions from other multivacancy states produced in the photoionization process. Additional vacancy states that are likely to be produced are identified using shake calculations, and their Auger spectra are calculated using the MCDF method and compared with

the measured spectrum. The value of R is determined from the relative intensities of the K-$L_{2,3}L_{2,3}\,^1D$ diagram line and the KK-$KL_{2,3}L_{2,3}\,^2D$ hypersatellite line along with branching ratios into the final states from single- and double-K vacancies taken from experiment and theory. The measured R is compared with high-energy-limit calculations [9,10] and an empirical Z-scaling law [13].

II. EXPERIMENTAL METHODS

The threshold for double-K ionization of Ne is 1863 eV [17] compared with 870.21 eV for single-K ionization [5]. The energies and relative intensities of Ne K-LL Auger diagram lines and the satellite lines resulting from additional excitation or ionization of the L shell have been determined experimentally [5,19,20]. The calculated KK-KLL hypersatellites are located in the 813–879 eV kinetic-energy range [18], and are shifted up in energy from the corresponding diagram lines by $\approx$66 eV. The strongest predicted hypersatellite KK-$KL_{2,3}L_{2,3}\,^2D$ was recorded in recent electron-impact experiments [17] at 870.5(3) eV. Observation of hypersatellites in that experiment, and in an earlier electron-impact experiment [16], was complicated by the presence of a large background.

The present measurements were made using 5000 eV x rays on beam line 12-ID at Argonne's Advanced Photon Source [21]. The x-ray beam passed through an effusive gas jet of Ne that was maintained at a constant gas density by a flow control valve. Auger-electron spectra were recorded by a double-pass cylindrical mirror analyzer (CMA) [22] positioned with its cylinder axis perpendicular to the propagation direction and at 54.7° to the linear-polarization direction of the x-ray beam. At this position, the intensities of photoelectrons and Auger electrons integrated over the acceptance angles of the CMA are independent of dipole anisotropies and first-order nondipole asymmetries [23]. The electron energy scales of the Auger spectra were calibrated using the diagram line energies tabulated in Ref. [5].

A survey spectrum (Fig. 1) through the diagram lines and the energy region of the hypersatellite lines indicated that data could be recorded with a good signal-to-background ratio. The CMA was operated at 100 eV pass energy to provide sufficient resolution while retaining detection efficiency. The 795–895 eV region was scanned repeatedly to record the hypersatellites along with the K-$L_{2,3}L_{2,3}\,^1S$ and ^1D diagram lines (see Fig. 2). The electron counts were corrected for an estimated 12% variation of the detection efficiency over 795–895 eV due to variation of the CMA's source volume at constant pass energy [22]. Correction was also made for 5% variation in the x-ray flux determined from the photocurrents from isolated beryllium windows through which the beam passed. The correction was consistent with variations of the number of x rays scattered from the gas target, which were recorded by a NaI scintillation detector.

III. RESULTS AND DISCUSSION

A fit with Voigt functions to the K-$L_{2,3}L_{2,3}\,^1S$ and ^1D diagram peaks gave a full width at half maximum (FWHM)

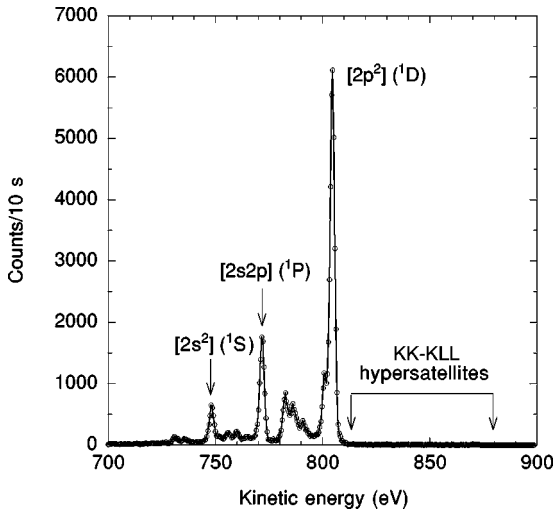

FIG. 1. The Auger-electron spectrum of Ne excited by absorption of 5000-eV x rays. Three prominent diagram lines resulting from decay of single-K vacancies are identified by their final states, and the energy region of the calculated KK-KLL hypersatellites is indicated.

of 2.59 eV. Even with that modest a resolution, the Lorentzian width from the fit was 0.25(6) eV, in agreement with the tabulated K-vacancy lifetime width of 0.27(2) eV [5]. A weak structure appears in the (830–880)-eV region when viewed on an expanded scale. The sloping background in this region is the Lorentzian tail of the K-$L_{2,3}L_{2,3}\,^1D$ diagram peak. Removal of the background gives the satellite structure plotted in Fig. 3 along with the calculated hypersatellite spectrum [18]. To account for instrumental resolution, the stick spectrum of Ref. [18] was broadened with a Voigt function obtained by fitting the KK-$KL_{2,3}L_{2,3}\,^2S$ and ^2D hypersatellite peaks between 860–875 eV. The ^2S hypersatellite is

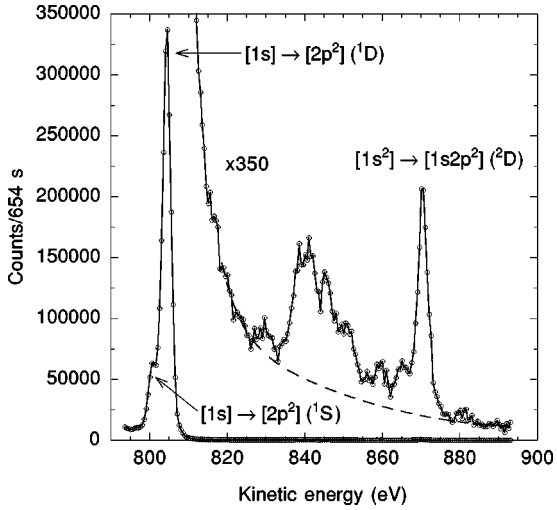

FIG. 2. The Auger-electron spectrum of Ne excited by absorption of 5000-eV x rays. The K-$L_{2,3}L_{2,3}\,^1S$ and ^1D diagram lines and the KK-$KL_{2,3}L_{2,3}\,^2D$ hypersatellite line are indicated. The structure between 830–860 eV is discussed in the text. The dashed curve beneath the peaks in the (820–890)-eV region is the estimated background and tail of the ^1D diagram peak.

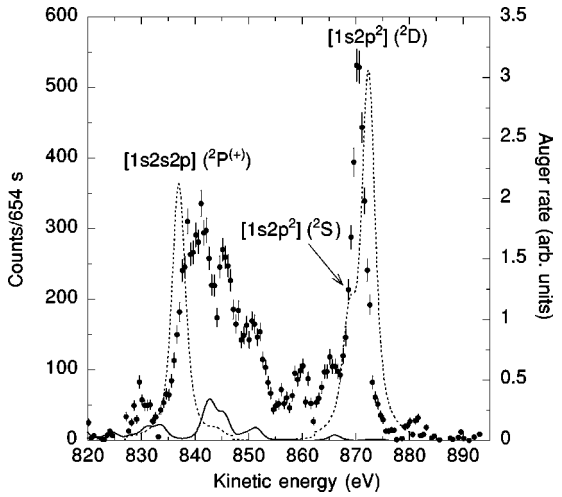

FIG. 3. Measured Auger spectrum (circles) compared with the calculated *KK-KLL* hypersatellite spectrum [18] (dotted curve) and the calculated contribution from $[1s2p]np$ and $[1s2s]ns$, $n=3$, 4 initial states (solid curve). The calculated hypersatellite spectrum is broadened by the experimental hypersatellite line shape, is arbitrarily scaled, and three strong transitions are identified by their final states. The calculated spectrum for $[1s2p]np$ and $[1s2s]ns$, $n=3$, 4 initial states is broadened by the experimental diagram line shape and is scaled to the measured spectrum by a procedure explained in the text.

weaker and more likely to be contaminated by transitions from other initial vacancy states that are discussed below. We report results only for the fit to the ^2D hypersatellite. The fitted position is 870.50(3) eV, in agreement with the measurements of Ref. [17] but 1.9 eV lower than the MCDF calculation. However, the calculated energy of the K-$L_{2,3}L_{2,3}$ ^1D diagram line is 806.78 eV, which is 2.30 eV higher than experiment [5]. So theory and experiment differ by only 0.4 eV for the energy difference between the KK-$KL_{2,3}L_{2,3}$ ^2D hypersatellite and the K-$L_{2,3}L_{2,3}$ ^1D diagram line. The Voigt fit to the hypersatellites gave a FWHM of 3.0 eV and a Lorentzian width of 1.0(1) eV. The Lorentzian width is consistent with the sum of the calculated double-K lifetime width (0.824 eV) [18] and the measured single-K lifetime width [0.27(2) eV] [5].

A. Initial vacancy states

The measured structure between 830–860 eV is only partly explained by the calculation [18], suggesting that initial vacancy states are produced in addition to $[1s^2]$ (in the following, we use the notation $[AB]CD$ to represent configurations with vacancies in the A and B subshells and excited electrons in the C and D subshells). In an experiment using both electron- and photon-impact excitations of Ne, Krause *et al.* [19] identified Auger satellites in the $\approx$(830–880)-eV region attributed to initial states of the type $[1s2p]np$ and $[1s2s]ns$. These states are shakeup satellites of $[1s]$ vacancies and can be observed directly in x-ray photoelectron spectra [24]. We estimated the contributions of these initial states to our measured Auger spectrum as follows. In the x-ray photoelectron spectrum of Ref. [24], the four strongest $[1s2p]np$ satellites are $[1s2p](^3P)np(^2S)$ and $[1s2p](^1P)np(^2S)$ with $n=3$, 4. The four strongest $[1s2s]ns$ satellites are $[1s2s](^3S)ns(^2S)$ and $[1s2s](^1S)ns(^2S)$ with $n=3$, 4. MCDF calculations similar to those in Ref. [18] were performed to generate Auger spectra for the eight initial states. To account for lifetime widths and instrumental resolution, the theoretical spectra were broadened with the Voigt function obtained by fitting the K-$L_{2,3}L_{2,3}$ ^1S and ^1D diagram peaks in Fig. 2. The amplitudes of the calculated spectra were scaled to the measured amplitude of the K-$L_{2,3}L_{2,3}$ ^1D peak in Fig. 2 using the intensities of the shakeup initial states relative to $[1s]$ vacancies measured using 1487-eV x rays [24] and branching-ratio measurements from $[1s]$ vacancies into diagram Auger lines obtained using 40-keV electron impact [20]. We assumed that the probabilities for decay into single-Auger final states, as compared with multiple-Auger and fluorescence channels, are the same for the shakeup initial states as for $[1s]$ vacancies [25]. The sum of the eight scaled Auger spectra is compared with the measured spectrum in Fig. 3, where they are seen to account for roughly 20% of the measured intensity. Additional initial states, therefore, apparently make significant contributions to the measured spectrum. From the relative intensities reported in Ref. [24], we estimate that the eight shakeup states included in our procedure account for $\approx$80% of the shakeup intensity in the Ne $1s$ photoelectron spectrum. The shakeoff states $[1s2p]$ and $[1s2s]$ produce Auger lines at kinetic energies well below the hypersatellite region [19,20].

Shake calculations were performed to identify at least some of the multivacancy states that are produced by photoionization in addition to $[1s^2]$. Single-configuration Hartree-Fock wave functions were calculated for the Ne ground state and vacancy states and represented by linear combinations of determinantal functions. We consider states having the same $^2S^e$ symmetry as the $[1s]$ vacancy state. Continuum orbitals of appropriate symmetries were calculated for states in which additional electrons are shaken off. The shake probability to a nine-electron state χ is given by the overlap integral $|\langle[1s]_{gs}|\chi\rangle|^2$, where the $[1s]_{gs}$ state consists of the unrelaxed orbitals of the ground state, but with a vacancy in the K shell. This describes the probability that, given the sudden removal of a $1s$ electron, the remaining electrons relax to an eigenstate χ of the ionic Hamiltonian. Using the single-configuration wave functions restricts the excited electrons to bound or continuum orbitals of s or p symmetry due to the single-particle angular overlaps from the ground state. We calculate the shake probability for $[1s^2]$ to be 3.04×10^{-4}, compared with 8.7×10^{-4} calculated in Ref. [9] using a highly correlated ground state for He-like Ne. Table I lists our results for relative shake probabilities scaled to 100% for $[1s^2]$. Our results show a probability of 0.61 for an additional $2p$ excitation or ionization, relative to that of pure $[1s^2]$ excitation. This is in comparison with a value of 0.46 calculated by Smit *et al.* [16], who ascribe the intensity to shakeoff of one or more $2p$ electrons. The Z-scaling laws [8] indicate that double-K photoionization of Ne at 5000 eV is below the high-energy-limit regime, so knockout is expected to affect the relative yields of vacancy states. Given the limi-

TABLE I. Results of shake calculations for the relative intensities of double-K-vacancy states of Ne.

Vacancy state	Intensity
$[1s^2]3s(^2S)$	5
$[1s^2]ns(^2S), n>3$	2
$[1s^2](^2S)$	100
$[1s^22p]np(^3S)$	0
$[1s^22p]3p(^1S)$	37
$[1s^22p]4p(^1S)$	7
$[1s^22p]np(^1S), n>4$	7
$[1s^22p](^2P)$	10
$[1s^22s]3s(^3S)$	70
$[1s^22s]4s(^3S)$	20
$[1s^22s]ns(^3S), n>4$	23
$[1s^22s]3s(^1S)$	8
$[1s^22s]4s(^1S)$	3
$[1s^22s]ns(^1S), n>4$	3
$[1s^22s](^2S)$	5
$[1s^22p]ns(^{1,3}P)$	2

tations of our model, the relative intensities in Table I are used simply to identify vacancy states that are likely to be produced along with $[1s^2]$.

MCDF calculations were performed to generate Auger spectra for several of the initial states listed in Table I. The calculated lines were broadened by the Voigt function determined in fitting the measured hypersatellite peaks between 860–875 eV. The calculated spectra for five initial states are compared on arbitrary scales with the measurement in Fig. 4. The $[1s^22p]3p(^1S)$ and $[1s^22s]3s(^3S)$ initial states [Fig. 4(a)] are predicted to be the two strongest ones, in which an L-shell electron is shaken up in addition to the removal of both K-shell electrons. They produce Auger lines at energies below the measured 870.5-eV peak that we attribute to the KK-$KL_{2,3}L_{2,3}\,^2D$ transition. Correction for the calculated energy of the K-$L_{2,3}L_{2,3}\,^1D$ diagram line would lower their energies by 2.3 eV. While these shakeup initial states are likely to contribute to the measured spectrum in the $\approx$(850–870)-eV region, the detailed shapes of the predicted spectra are not apparent, indicating that their contributions are smaller relative to $[1s^2]$ than is suggested by the intensities in Table I. The calculated spectrum for the $[1s^2]3s(^2S)$ initial state [Fig. 4(a)] has its strongest peak at the very weak experimental bump near 881 eV. Figure 4(b) shows the calculated spectra for the $[1s^22p](^2P)$ and $[1s^22s](^2S)$ initial states in which an L-shell electron is shaken off in addition to the removal of both K-shell electrons. These initial states produce Auger lines in the $\approx$(840–860)-eV region and likely account for some of the measured intensity that is not explained by the $[1s^2]$ and $[1s2p]np$ and $[1s2s]ns$ initial states (see Fig. 3).

Combining a shake calculation to identify initial vacancy states with MCDF calculations of their Auger spectra indicates that the measured spectrum consists of several contributions, but we are unable to attain a definitive analysis of their relative weights. A more extensive calculation that incorporates electron correlation in the ground state and ionic states is required to obtain quantitative estimates of relative intensities, even in the sudden approximation (see, e.g., Ref. [26]). Beyond that, knockout is expected to be important at the experimental energy used. While it is likely that some of the measured intensity near the 870.5-eV peak is due to transitions other than the KK-$KL_{2,3}L_{2,3}\,^2D$ hypersatellite, the fitted energy and width of that peak are consistent with the MCDF calculations. We therefore proceed under the assumption that the fitted area of that peak is due to that transition alone.

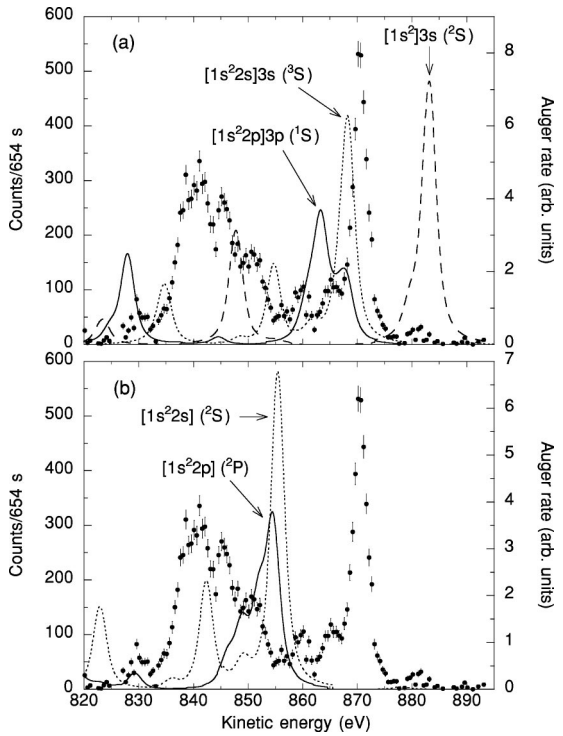

FIG. 4. Measured Auger spectrum (circles) compared with calculated spectra from five initial states with empty K shells. The initial states in (a) are $[1s^22p]3p(^1S)$ (solid curve), $[1s^22s]3s(^3S)$ (dotted curve), and $[1s^2]3s(^2S)$ (dashed curve). The initial states in (b) are $[1s^22p](^2P)$ (solid curve) and $[1s^22s](^2S)$ (dotted curve). The calculated spectra are broadened by the experimental hypersatellite line shape and are arbitrarily scaled.

B. Double-to-single K-shell photoionization ratio

From the fitted Voigt functions, we determine the intensity ratio of the KK-$KL_{2,3}L_{2,3}\,^2D$ hypersatellite to the K-$L_{2,3}L_{2,3}\,^1D$ diagram line to be 0.002 23(10). When vacancies are produced by (4.5–5)-keV electron impact [16,17,19], this ratio is measured to be much smaller $\approx$0.0004 (see Fig. 3 of Ref. [17]). While this ratio is measured at the specific energy of 5000 eV in the present photoionization experiment, the electron-impact measurements comprise an average over a range of energy transfers from the $[1s^2]$ threshold up to the beam energy. The difference of a factor of 5–6 for the hypersatellite-to-diagram intensity ratio between photon and electron impact suggests that the

electron-impact measurements sample the rising edge of the double-*K* photoionization cross section rather than the broad maximum [7,8]. While this seems to be the case for double-*K*-vacancy production, the experiment of Ref. [27] showed that production of $KL^x(x=1,2,\ldots)$ multiple vacancies in Ne by 1.5-keV x rays and by 3.2-keV electron impact was essentially the same. This is consistent with our result in Fig. 3, that is, the Auger lines from $[1s2p]np$ and $[1s2s]ns$ vacancy states account for only $\approx 20\%$ of the intensity in the energy region of the *KK* hypersatellites, i.e., the *KL* shakeup states contribute roughly the same intensities relative to single-*K* vacancies in both the present 5-keV photoionization experiment and the (4.5–5)-keV electron-impact experiments, but double-*K* vacancies are produced a factor of ≈ 5 times stronger in the photoionization experiment. In a 10-keV electron-impact experiment in which the Ne *KK*-*KL* x-ray fluorescence hypersatellite was recorded, the *KK* shakeoff probability was estimated to be 0.001 [28].

To determine the double-to-single *K*-shell photoionization cross section ratio *R* from the hypersatellite-to-diagram line intensity ratio, the branching ratios from $[1s^2]$ and $[1s]$ vacancies into the respective final states are needed. Recently, the relative yields of Ne^{1+}–Ne^{4+} ions were measured in coincidence with $1s$ photoelectrons [25]. The coincidence method excludes contributions from other initial vacancy states such as those with additional excitation or ionization of the *L* shell. The yields are interpreted as determining the branching ratios for a $[1s]$ vacancy into fluorescence and single-, double-, and triple-Auger decay channels. The yield for Ne^{2+} was 0.9267(21), showing the dominance of single-Auger decay. In the same paper [25], the probabilities of double-Auger processes were calculated for both shakeup and shakeoff of additional *L*-shell electrons. Shakeoff produces Ne^{3+} and shakeup also leads to Ne^{3+} in many cases due to stepwise double-Auger decay. Only a fraction of double-Auger processes contribute to the Ne^{2+} yield. It was also noted that shakeoff upon radiative decay, which also produces Ne^{2+}, can be neglected. Hence, to a good approximation, the Ne^{2+} yield can be attributed to diagram Auger decays. Among the diagram Auger lines, the branching ratio for K-$L_{2,3}L_{2,3}\,{}^1D$ has been measured to be 0.6086(15) [20]. Using this branching ratio along with the Ne^{2+} yield per $[1s]$ vacancy from Ref. [25], the relative number of $[1s]$ vacancies produced in the present experiment is determined from the area of the K-$L_{2,3}L_{2,3}\,{}^1D$ peak in Fig. 2.

The branching ratios for decay of $[1s^2]$ vacancies are not known experimentally, but the single-Auger decay rates and fluorescence yield were calculated in Ref. [18]. The calculated fluorescence yield increases by 33% compared with that for $[1s]$ vacancies. From Ref. [25], the combined yields of fluorescence and double- and triple-Auger decay for a $[1s]$ vacancy are 0.0731(35). If these yields are as much as twice as great for $[1s^2]$ vacancies, the single-Auger yield would be ≈ 0.85. We therefore estimate the single-Auger yield for $[1s^2]$ vacancies to be 0.90(5), with the large uncertainty reflecting the lack of knowledge of the actual yield. Using that yield along with the calculated single-Auger branching ratio of 0.440 for the KK-$KL_{2,3}L_{2,3}\,{}^2D$ hypersatellite, we determined the relative number of $[1s^2]$ vacancies produced from its peak area in Fig. 2.

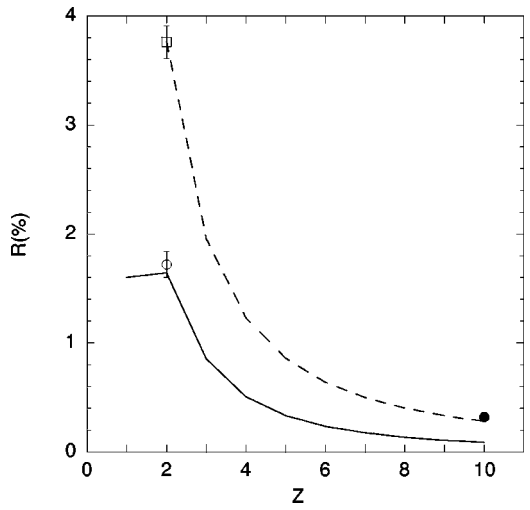

FIG. 5. Ratio of double-to-single *K*-shell photoionization cross sections measured for He at 5.4–9.1 keV (open circle) [11], He at 190 eV (open square) [1], and Ne at 5 keV (closed circle) compared with results of high-energy-limit calculations on He-like systems (solid curve) [9] and an empirical *Z*-scaling law (dashed curve) [13].

Combining our measured intensity ratio of the hypersatellite to the diagram line with the single-Auger yields and branching ratios, we obtain $R=0.32(4)\%$. This result is plotted in Fig. 5 along with measurements on He at high energy (5.4–9.1 keV) [11] and at 190 eV [1] where the *R* value for He reaches its maximum. The measurements are compared with the high-energy-limit calculations for He-like systems [9]. A similar calculation was reported in Ref. [10]. It should be noted that the calculated *R* values are for the ratio of double ionization to the sum of single ionization and single ionization plus excitation, while the present measurement on Ne determines the ratio of double ionization to single ionization and excludes single ionization plus excitation. However, for $Z=10$ the calculations of Ref. [10] show that exclusion of single ionization plus excitation increases the asymptotic ratio only slightly from 0.087% to 0.0871%, so the comparison in Fig. 5 remains valid. While the high-energy measurement on He agrees with the calculated asymptotic ratio, the He measurement at 190 eV is larger by a factor of ≈ 2 and the present result for Ne at 5000 eV is larger than the calculated ratio by a factor of ≈ 4. The experimental *R* values for higher-*Z* atoms determined from intensity ratios of x-ray fluorescence hypersatellites to diagram lines [12–15] are also larger than the high-energy-limit calculations. In these cases and for Ne at 5000 eV and He at 190 eV, the photon energies used are within the broad maximum of the double-*K* photoionization cross section calculated by *Z* scaling [8], where knockout is an important interaction. An empirical *Z*-scaling law was determined in Ref. [13] by fitting *R* values measured at energies where knockout is important, including the He measurement at 190 eV. This empirical curve is plotted in Fig. 5 and gives $R=0.28(3)\%$ for Ne, in good agreement with the present measurement. A compari-

son of the empirical and asymptotic curves in Fig. 5 thus gives a rough estimate of the effect of knockout relative to shakeoff.

IV. CONCLUSION

Double *K*-shell photoionization of Ne at 5000 eV was observed by recording the *KK*-*KLL* Auger hypersatellite spectrum. The measured spectrum is complicated by contributions from other initial vacancy states, e.g., double-*K* ionization plus excitation or ionization of the *L* shell. Shake calculations were used to identify the likely initial vacancy states, and their Auger spectra were calculated by the MCDF method and compared with the measured spectrum. The measured intensity ratio of the KK-$KL_{2,3}L_{2,3}\,^2D$ hypersatellite to the K-$L_{2,3}L_{2,3}\,^1D$ diagram line was combined with experimental and theoretical data on branching ratios from single- and double-*K* vacancies to determine the double-to-single *K*-shell photoionization cross-section ratio. The measured ratio is much larger than the calculated high-energy-limit value, indicating that knockout is an important interaction for double *K*-shell photoionization of Ne at 5000 eV. This experiment illustrates the difficulty of using Auger spectra to determine double-*K* photoionization cross sections. There are remaining ambiguities in the assignment of the Auger spectrum that could be investigated in future studies. Inclusion of knockout interactions in future calculations of energy-dependent double-*K* photoionization cross sections is also needed.

ACKNOWLEDGMENTS

We are grateful to the staff of the Basic Energy Sciences Synchrotron Radiation Center at the Advanced Photon Source for their assistance in performing the experiments. We thank Uwe Arp for preliminary estimates of shake probabilities. The Argonne group was supported by the Chemical Sciences, Geosciences, and Biosciences Division of the Office of Basic Energy Sciences, Office of Science, U.S. Department of Energy, under Contract No. W-31-109-ENG-38. G.B.A., J.C.L., and D.L.E. were supported by the National Science Foundation. The work of M.H.C. was performed under the auspices of the U.S. Department of Energy by the University of California Lawrence Livermore National Laboratory under Contract No. W-7405-ENG-48. Use of the Advanced Photon Source was supported by the U.S. Department of Energy, Basic Energy Sciences, Office of Science, under Contract No. W-31-109-ENG-38.

[1] J.A.R. Samson, W.C. Stolte, Z.-X. He, J.N. Cutler, Y. Lu, and R.J. Bartlett, Phys. Rev. A **57**, 1906 (1998).
[2] J.H. McGuire, N. Berrah, R.J. Bartlett, J.A.R. Samson, J.A. Tanis, C.L. Cocke, and A.S. Schlachter, J. Phys. B **28**, 913 (1995).
[3] H.R. Sadeghpour, Can. J. Phys. **74**, 727 (1996).
[4] K. Hino, T. Ishihara, F. Shimizu, N. Toshima, and J.H. McGuire, Phys. Rev. A **48**, 1271 (1993).
[5] V. Schmidt, *Electron Spectrometry of Atoms using Synchrotron Radiation* (Cambridge University, Cambridge, 1997).
[6] R.C. Forrey, Z.-C. Yan, H.R. Sadeghpour, and A. Dalgarno, Phys. Rev. Lett. **78**, 3662 (1997).
[7] T. Schneider, P.L. Chocian, and J.-M. Rost, Phys. Rev. Lett. **89**, 073002 (2002).
[8] M.A. Kornberg and J.E. Miraglia, Phys. Rev. A **49**, 5120 (1994).
[9] R.C. Forrey, H.R. Sadeghpour, J.D. Baker, J.D. Morgan, III, and A. Dalgarno, Phys. Rev. A **51**, 2112 (1995).
[10] R. Krivec, M.Y. Amusia, and V.B. Mandelzweig, Phys. Rev. A **63**, 052708 (2001).
[11] L. Spielberger *et al.*, Phys. Rev. Lett. **74**, 4615 (1995).
[12] J. Ahopelto, E. Rantavuori, and O. Keski-Rahkonen, Phys. Scr. **20**, 71 (1979).
[13] E.P. Kanter, R.W. Dunford, B. Krässig, and S.H. Southworth, Phys. Rev. Lett. **83**, 508 (1999).
[14] R. Diamant, S. Huotari, K. Hämäläinen, C.C. Kao, and M. Deutsch, Phys. Rev. A **62**, 052519 (2000).
[15] M. Oura *et al.*, J. Phys. B **35**, 3847 (2002).
[16] Ž. Šmit, M. Žitnik, L. Avaldi, R. Camilloni, E. Fainelli, A. Mühleisen, and G. Stefani, Phys. Rev. A **49**, 1480 (1994).
[17] P. Pelicon, I. Čadež, M. Žitnik, Ž. Šmit, S. Dolenc, A. Mühleisen, and R.I. Hall, Phys. Rev. A **62**, 022704 (2000).
[18] M.H. Chen, Phys. Rev. A **44**, 239 (1991).
[19] M.O. Krause, T.A. Carlson, and W.E. Moddeman, J. Phys. (Paris) **32**, C4-139 (1971).
[20] A. Albiez, M. Thoma, W. Weber, and W. Mehlhorn, Z. Phys. D: At., Mol. Clusters **16**, 97 (1990).
[21] M.A. Beno, G. Jennings, M. Engbretson, G.S. Knapp, C. Kurtz, B. Zabransky, J. Linton, S. Seifer, C. Wiley, and P.A. Montano, Nucl. Instrum. Methods Phys. Res. A **467-468**, 690 (2001).
[22] P.W. Palmberg, J. Vac. Sci. Technol. **12**, 379 (1975).
[23] M. Jung, B. Krässig, D.S. Gemmell, E.P. Kanter, T. LeBrun, S.H. Southworth, and L. Young, Phys. Rev. A **54**, 2127 (1996).
[24] S. Svensson, B. Eriksson, N. Mårtensson, G. Wendin, and U. Gelius, J. Electron Spectrosc. Relat. Phenom. **47**, 327 (1988).
[25] B. Kanngießer *et al.*, Phys. Rev. A **62**, 014702 (2000).
[26] K.G. Dyall, J. Phys. B **16**, 3137 (1983).
[27] M.O. Krause, F.A. Stevie, L.J. Lewis, T.A. Carlson, and W.E. Moddeman, Phys. Lett. **31A**, 81 (1970).
[28] H. Ågren, J. Nordgren, L. Selander, C. Nordling, and K. Siegbahn, J. Electron Spectrosc. Relat. Phenom. **14**, 27 (1978).